Contents lists available at ScienceDirect

Transactions of Nonferrous Metals Society of China

36(2026) 649−658

www.tnmsc.cn

Volatilization kinetics and mechanisms of arsenic during vacuum distillation

Lin ZOU [a,b,c], Guo-long CHEN [a,b], Guo-zheng ZHA [a,b,*], Wen-long JIANG [a,b], Bao-qiang XU [a,b], Bin YANG [a,b], Da-chun LIU [a,b,**]

[a] National Engineering Research Center of Vacuum Metallurgy, Kunming University of Science and Technology, Kunming 650093, China;

[b] Faculty of Metallurgical and Energy Engineering, Kunming University of Science and Technology, Kunming 650093, China;

[c] Shandong Humon Smelting Co., Ltd., Yantai 264000, China

Abstract: The volatilization characteristics and kinetic mechanisms of arsenic were investigated in the temperature range of 623−773 K and pressure ranges of 10−10000 Pa. The experimental results reveal that the evaporation rate increases with increasing temperature and decreasing pressure. Surface reaction control dominates at low pressures (<100 Pa), whereas diffusion control dominates at high pressures (>5000 Pa). The evaporation behavior is successfully described by an Arrhenius-type model for temperature dependence and Logistic model for pressure dependence. Key kinetic parameters, including the critical pressure, maximum evaporation rate and evaporation coefficient, were calculated. The evaporation coefficient varies between 0.010 and 0.223, and the critical pressures vary between 281 and 478 Pa with temperature.

Keywords: arsenic; vacuum distillation; evaporation rate; kinetic modeling; process optimization

1 Introduction

Arsenic plays a critical role in various industrial applications, including semiconductor manufacturing, wood preservatives, and alloying agents [1−3]. However, arsenic is highly toxic, and stringent purification processes are required to minimize both environmental and human health risks [4,5]. Industrial arsenic typically exists in an impure form and is recovered from arsenic-rich smelter dust, which often contains significant levels of impurities such as sulfur, lead, copper, and selenium [6−8]. Currently, vacuum distillation is recognized as an efficient and environmentally friendly technique for refining crude arsenic [9]. Arsenic can be vaporized at relatively low temperatures, whereas other impurities, which have much lower vapor pressures, remain in the residue; thus, this process achieves purification. With this method, crude arsenic with a purity of 95%−98% or an As-based alloy can be refined to pure arsenic (As ≥99.9%) [10−13]. Arsenic can also be removed from various complex materials via vacuum distillation through its volatility. YANG et al [14] used a vacuum reduction method to remove arsenic from arsenic-containing polymetallic materials and achieved a removal rate greater than 96%. ZHANG et al [11] employed a vacuum gasification−directional condensation method to remove arsenic impurities from crude tin, with both arsenic removal rates and tin recovery rates exceeding 99%. Although considerable research has focused on process optimization involving temperature, pressure, and operation time, most of

Corresponding author: *Guo-zheng ZHA, Tel: +86-18487375302, E-mail: gz_zha@kust.edu.cn;
**Da-chun LIU, Tel: +86-13608858239, E-mail: kmustdcl@163.com

https://doi.org/10.1016/S1003-6326(25)66988-3
Received 21 January 2025; accepted 27 October 2025

these studies remain empirical and lack systematic investigations into the volatilization kinetics and fundamental evaporation mechanisms.

Previous studies have shown that the volatilization behavior of metals such as antimony and selenium under vacuum conditions is closely related to their kinetic characteristics. For example, the volatilization behavior of elemental antimony under vacuum conditions was investigated at different temperatures (973−1473 K) and pressures (5−500 Pa), and the results revealed that the evaporation rate of antimony had a linear relationship with temperature and followed a logistic model with pressure [15,16]. Similarly, the evaporation kinetics of lead, silver, and their alloys revealed that the evaporation rate linearly increased with temperature and exponentially decreased with pressure, and important insights for optimizing vacuum separation processes were obtained [17]. The volatilization of elemental selenium exhibited three-stage behavior with a critical pressure point, highlighting the complexity of its volatilization kinetics and providing a basis for efficient selenium separation [18]. Despite the widespread use of vacuum distillation for arsenic purification or arsenic removal from various secondary resources, the fundamental mechanisms governing its volatilization behavior have been inadequately explored [19,20].

To address these gaps, in this study, the volatilization behavior and kinetic mechanisms of arsenic under various vacuum distillation conditions were investigated, and experimental measurements and theoretical modeling were combined to establish quantitative kinetic parameters for process optimization.

2 Experimental

2.1 Materials and equipment

As shown in Fig. 1(a), high-purity arsenic (99.99%), which was obtained from an industrial smelting process at Shandong Humon Smelting Co., Ltd., China, was used to ensure the accuracy and reproducibility of the experimental results. As shown in Fig. 1(b), a vacuum differential mass analyzer was used for the experiments and could accurately determine the changes in the metal mass and pressure during the vacuum distillation process.

The apparatus was equipped with a high-precision temperature and pressure controller, and the distilled temperature and system pressure fluctuations were accurately controlled. The measurement accuracies for the mass, pressure and temperature were 0.001 g, 0.1 Pa and ±1 K, respectively. The system could read 50 data points per second, ensuring high reliability of the collected data. The crucible material was selected for its thermal stability and inertness to arsenic under the experimental conditions, and the volatilization surface area of the crucible was 7.065 cm^2 throughout the experiment. A condensation device was installed above the crucible to ensure that all the arsenic vapor was condensed. The mass changes of arsenic over time under different temperatures and pressures were measured experimentally, and the evaporation rate of arsenic (ω) was calculated on the basis of its definition, as shown in Eq. (1):

$$\omega = \frac{\Delta m(t)}{\Delta t \cdot S} \tag{1}$$

where Δm represents the mass change, Δt represents the time interval, and S represents the evaporation area.

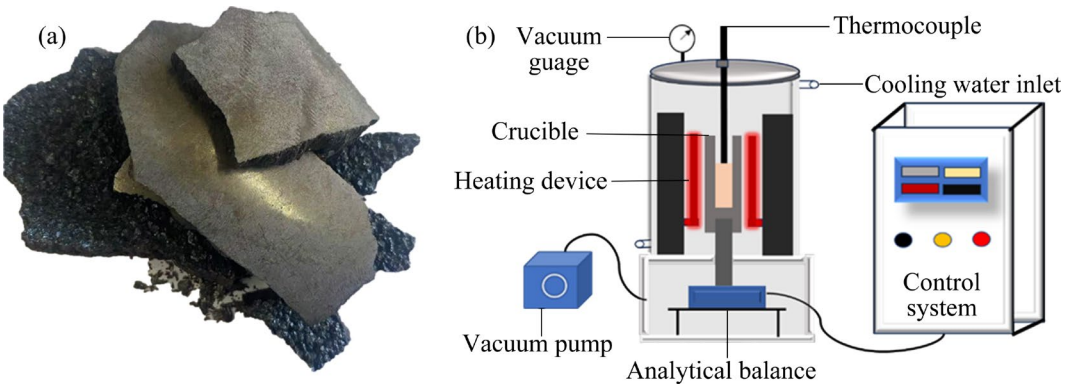

Fig. 1 (a) High-purity arsenic raw material and (b) vacuum differential gravity furnace

2.2 Experimental setup

Approximately 30 g of high-purity arsenic was weighed and placed in a high-purity graphite crucible. Vacuum distillation experiments were performed at various temperatures and pressures to comprehensively investigate the volatilization behavior of arsenic. The selected temperature range was 623−773 K, and this range was representative of industrial distillation conditions. The pressure varied from 10 to 10000 Pa to cover a wide range of vacuum conditions, which enabled the identification of critical pressure points that significantly affect the evaporation rate. Before heating, argon gas was emitted into the furnace three times to ensure that all the air was completely displaced and discharged to prevent arsenic oxidation during heating. The sample was heated at a controlled rate of 10 K/min until the designated temperature was reached and stable, and the vacuum system was activated to achieve the desired pressure level. The system was then held at the set temperature and pressure until the mass change of the sample stabilized; this process ensured that equilibrium conditions were reached. The mass of the sample and the temperature and pressure of the system were recorded in real time, and the data collection frequency was 50 readings per second to capture the transient changes effectively. Each experiment was conducted for a maximum duration of 5 min at a stable target system temperature and pressure to ensure sufficient data collection for kinetic analysis. This real-time monitoring enabled the precise determination of the evaporation rates and ensured that all critical points in the volatilization process were accurately captured. After the distillation was completed, the system was gradually cooled under controlled conditions to prevent the diffusion of arsenic vapor, and the condensed arsenic was collected from the cooler surfaces.

2.3 Experimental data analysis methods

In the experiment, the evaporation rates were determined on the basis of the mass loss of arsenic over time, the data were measured at various temperatures and pressures, and the differential method was used to calculate the evaporation rate to determine the volatilization behavior of the sample at different pressures. Anomalies in the mass change were observed during the experiment; to ensure the reliability of the original data, a systematic statistical analysis was conducted. The recorded mass loss data were initially screened using boxplots to identify and remove the outliers caused by system instability, vacuum fluctuations, and measurement noise. The original data were divided into 50 intervals (5 s per interval). For each segment, the local slope ($\Delta m/\Delta t$) was calculated and used to determine the instantaneous evaporation rate using Eq. (1). For each temperature and pressure, the slope data were analyzed to calculate the mean and standard deviation after abnormal values were excluded. The 95% confidence interval was used to assess the reliability and stability of the evaporation rate data. The Shapiro−Wilk and Kolmogorov−Smirnov tests were applied to verifying the normal distribution of the slope data. For data sets that did not meet the normality criteria, square root transformations were performed to ensure valid statistical evaluation. The slope value corresponding to the normalized mean served as the overall parameter estimate ($\Delta m/\Delta t$) to calculate accurate evaporation rate.

3 Results and discussion

3.1 Determination of evaporation rate of arsenic

The mass loss of the arsenic samples is recorded at various temperatures and pressures during the vacuum distillation experiments, as shown in Fig. 2. The results clearly indicate a trend of mass reduction with time, and this trend shows significant variability contingent on the experimental conditions. At lower pressures and higher temperatures, the mass loss rate is substantially greater, indicating the increased volatility of arsenic under these conditions. Figures 2(a−d) show the variation in the arsenic mass over time at different pressures but at a constant temperature. On the basis of these results, lower pressures result in more pronounced mass reduction, indicating increased evaporation rates. At 10 and 50 Pa, the mass of arsenic decreases at a significantly faster rate than at higher pressures, such as 5000 and 10000 Pa. These results indicate that lower pressures facilitate the evaporation of arsenic by reducing the resistance from the surrounding atmosphere, allowing arsenic atoms to transition more readily to the vapor phase. Additionally, the increase in temperature from 623 to 773 K accelerates this mass reduction, highlighting the importance of both temperature and pressure in controlling the evaporation rates. Similarly, Figures 3(e−j) present the mass variation of arsenic over time at a fixed pressure with varying

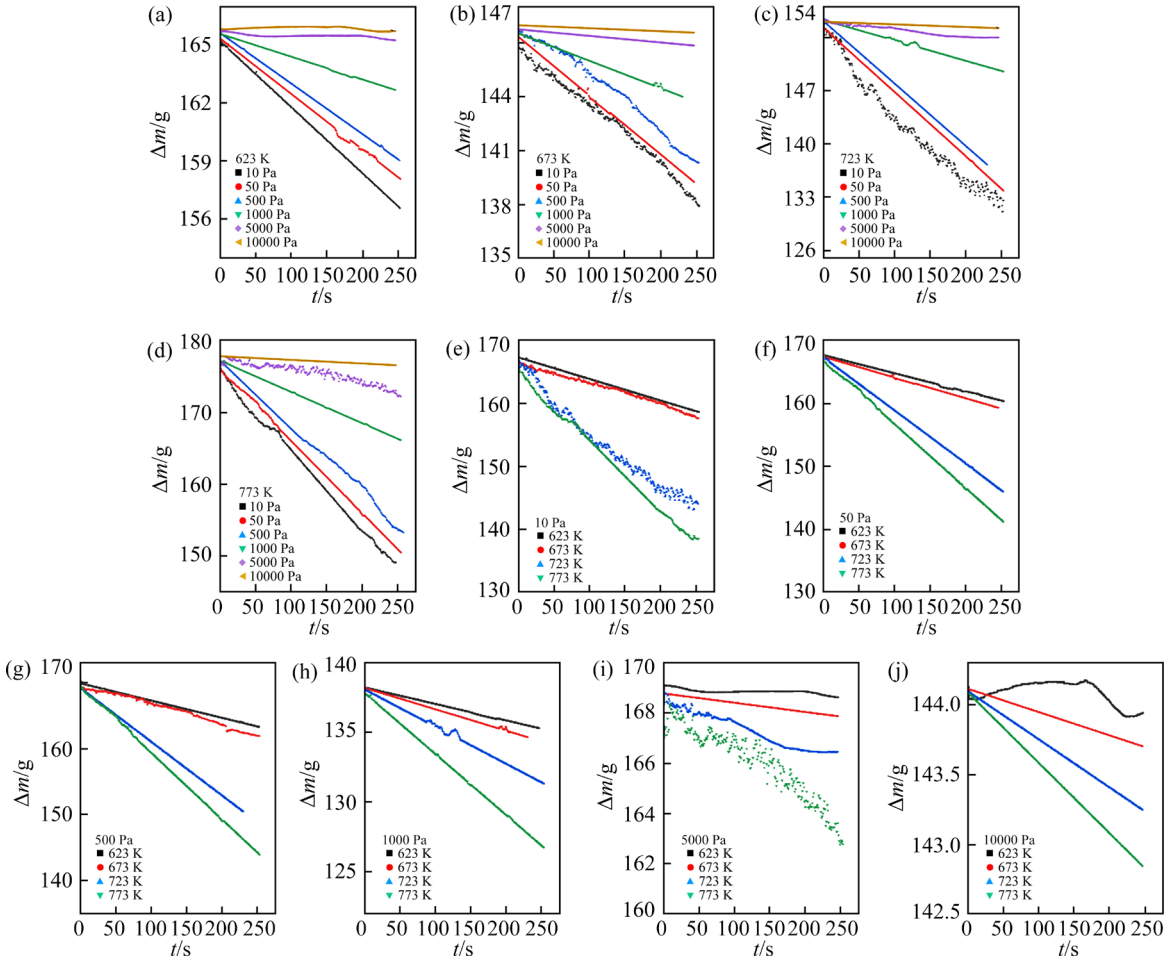

Fig. 2 Material mass variation over time at different temperatures and pressures: (a) 623 K; (b) 673 K; (c) 723 K; (d) 773 K; (e) 10 Pa; (f) 50 Pa; (g) 500 Pa; (h) 1000 Pa; (i) 5000 Pa; (j) 10000 Pa

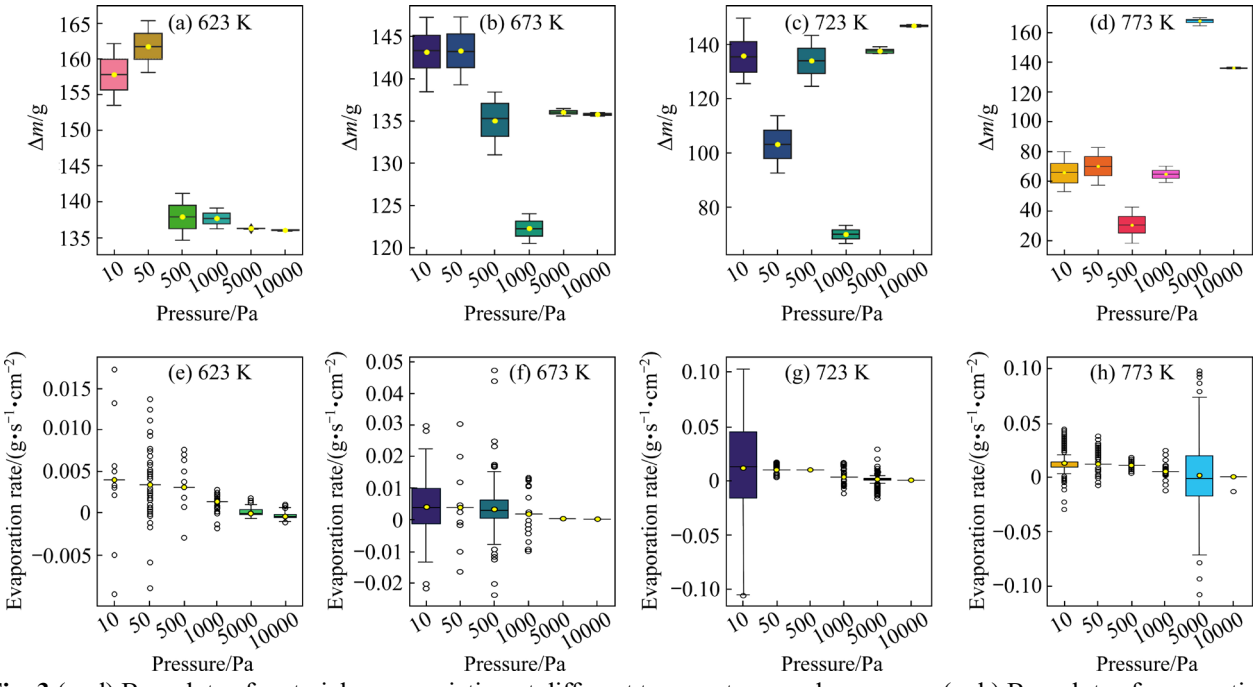

Fig. 3 (a−d) Box plots of material mass variation at different temperatures and pressures; (e−h) Box plots of evaporation rates at different temperatures and pressures

temperature. These findings reveal that the evaporation rate is significantly affected by temperature. Higher temperatures result in an increased rate of mass loss, and the sharpest decrease is observed at 773 K. This finding is attributed to the greater kinetic energy of the arsenic atoms at elevated temperatures, which facilitates their transition from the condensed phase to the vapor phase. A comparison of different temperatures at the same pressure clearly reveals that temperature plays a critical role in determining the efficiency of the distillation process.

To ensure the accuracy of the data used to calculate the evaporation rate, mathematical statistics is used to filter and statistically analyze the experimental data shown in Fig. 2, and the results are shown in Figs. 3(a−d). The box plots at 623, 673, 723, and 773 K under various pressure conditions reveal the significant effect of temperature and pressure on the volatilization behavior of metals. The variation in different distillation temperatures results in a more dispersed mass distribution of arsenic, and low pressures (such as 10−500 Pa) result in a more significant decrease in mass. These results indicate that low pressure is beneficial for accelerating the volatilization of arsenic. Higher pressures (such as 5000 and 10000 Pa) have inhibitory effects on volatilization. In addition, at lower temperatures, the data are more concentrated, indicating a stable volatilization process. At higher temperatures, the range of mass distribution increases significantly, and more outliers are observed, which indicates faster evaporation rates and greater process variability. After the filtered mass versus time data are obtained using box plots, the evaporation rate data points are segmented via Eq. (1), and a box plot of the evaporation rates at different temperatures and pressures is generated and plotted, as shown in Figs. 3(e−h). The evaporation rate decreases with increasing pressure across all temperatures, whereas higher temperatures significantly increase volatilization at low pressures. These factors result in increased mean values and broader distribution ranges. Overall, volatilization behavior is regulated by both temperature and pressure. At low pressure, temperature plays a dominant role, resulting in more intense volatilization. However, at high pressures, the suppression effect of pressure becomes predominant, and stable and negligible evaporation rates are attained. After the data are filtered, the actual evaporation rates of arsenic under different temperatures and pressures are calculated and given in Table 1.

Table 1 Evaporation rates of arsenic at different temperatures and pressures ($g\cdot s^{-1}\cdot cm^{-2}$)

Pressure/Pa	Temperature/K			
	623	673	723	773
10	4.10×10^{-3}	4.22×10^{-3}	1.13×10^{-2}	1.32×10^{-2}
50	3.44×10^{-3}	3.91×10^{-3}	1.00×10^{-2}	1.21×10^{-2}
500	3.12×10^{-3}	3.55×10^{-3}	9.73×10^{-3}	1.11×10^{-2}
1000	1.41×10^{-3}	1.83×10^{-3}	3.17×10^{-3}	5.29×10^{-3}
5000	2.30×10^{-4}	4.38×10^{-4}	1.17×10^{-3}	2.25×10^{-3}
10000	5.04×10^{-5}	1.99×10^{-5}	4.143×10^{-4}	5.44×10^{-4}

3.2 Relationship between evaporation rate of arsenic and temperature

The actual evaporation rates of arsenic (ω_{As}) listed in Table 1 are plotted as ω_{As} vs T and ln ω_{As} vs $1/T$, as shown in Figs. 4(a, b), respectively. As shown in Fig. 4(a), ω_{As} exhibits notable regularity as it varies with temperature and system pressure, and ω_{As} exhibits a significant nonlinear dependence on temperature, with a rapid exponential increase as the temperature increases. Across all pressures, a consistent trend of increasing evaporation rates with increasing temperature is observed. This phenomenon can be attributed to the additional thermal energy supplied by elevated temperatures, and this thermal energy facilitates the volatilization of arsenic molecules. At lower pressures (such as 10 and 50 Pa), the increase in the evaporation rate is particularly pronounced, especially within the temperature range from 673 to 723 K, where a rapid surge in volatility is observed. These results reveal the significant promoting effect of temperature on volatilization. As shown in Fig. 4(b), ln ω_{As} has a linear relationship with the reciprocal of the distillation temperature under constant pressure. This behavior indicates a thermally activated process that can be described by the Arrhenius equation:

$$\ln \omega_{As}=\ln A-E_a/(RT) \quad (2)$$

where A is the preexponential factor, 1/s; E_a is the activation energy, J/mol; T is the distilled temperature, K; R is the molar gas constant. The kinetic parameters A and E_a can be calculated by linearly fitting the slope and intercept at different

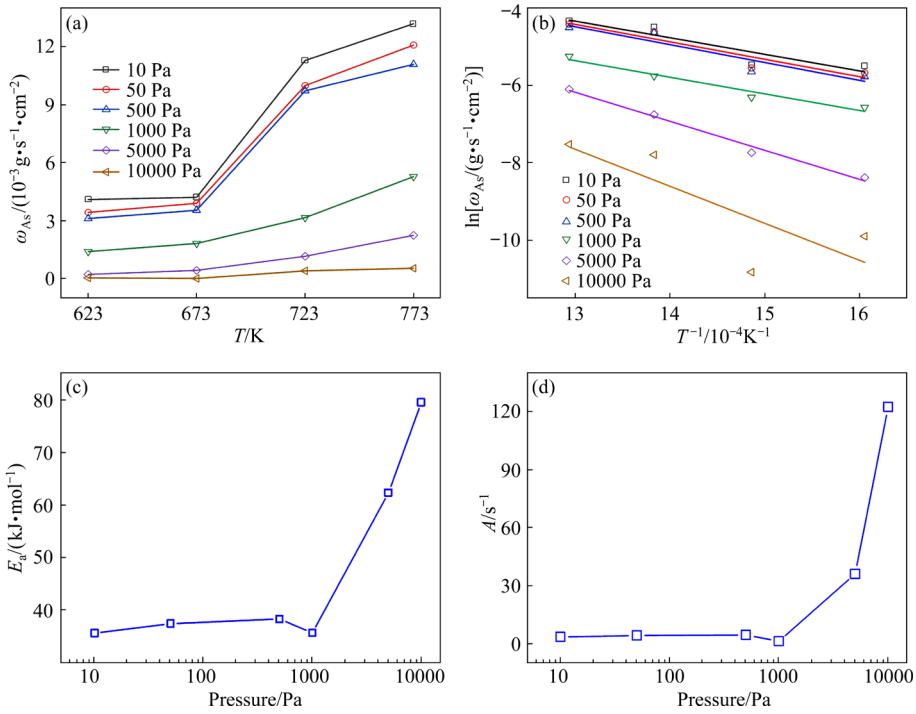

Fig. 4 (a) Plots of ω_{As} vs T at different system pressures, (b) plots of ln ω_{As} vs $1/T$ at different system pressures, (c) activation energy E_a at different pressures, and (d) preexponential factor A at different pressures

pressures, as shown in Fig. 4(c). E_a clearly remains relatively stable within the range of 35−38 kJ/mol, whereas A ranges from 1.2 to 4.5 s^{-1} at low pressures of 10−1000 Pa. These results indicate that the evaporation process is governed predominantly by surface-controlled physical adsorption and desorption at low pressure. The individual arsenic molecules detach from the solid or liquid phase and enter the vapor phase; therefore, temperature is the primary driver of the evaporation rate. At high pressures in range of 5000−10000 Pa, the dependence of the evaporation rate on temperature deviates from linear Arrhenius behavior and reveals more complex kinetic characteristics. These results indicate that the volatilization process at high pressures is no longer dominated solely by surface desorption but is affected by additional factors, including nonideal gas behavior, increased intermolecular interactions, and increased diffusion resistance. The substantial increase in E_a at high pressures likely represents the additional energy needed to overcome the molecular clustering or attractive forces in the gas phase. However, the increase in A indicates a transition to more complex dynamic behavior, potentially involving changes in surface activity or multimolecular interactions. Overall, the volatilization mechanism of arsenic indicates a distinct transition between the low-pressure regime and the high-pressure regime. At low pressures, the process is kinetically simple and surface controlled and is characterized by lower energy barriers. In contrast, high pressures result in significant complexities, where nonideal gas effects, diffusion limitations, and potential vapor-phase saturation collectively suppress the evaporation rate.

3.3 Relationship between evaporation rate of arsenic and pressure

The relationship between ω_{As} and system pressure is shown in Fig. 5(a). The overall trend of the arsenic evaporation rate clearly changes with temperature and pressure. ω_{As} increases as the system pressure decreases and as the distillation temperature increases. However, when the system pressure is reduced to a certain threshold, the evaporation rate reaches its maximum and remains nearly constant thereafter. In the low-pressure region (<100 Pa), the evaporation rate is highly dependent on temperature and nearly independent of pressure, exhibiting characteristics of the Langmuir surface reaction control mechanism. As the temperature increases, the evaporation rate rapidly increases, which indicates that the process in this region is primarily temperature driven and dominated by the

activation of surface reactions. In contrast, in the high-pressure region (>5000 Pa), the evaporation rate stabilizes, indicating a transition from surface reaction control to diffusion control. This result is consistent with the Fick diffusion mechanism. In this region, the evaporation rate becomes limited by gas-phase mass transfer, and further increases in pressure have a minimal effect. The intermediate pressure range (500−5000 Pa) represents a transitional zone for volatilization kinetics. Within this range, the contour lines gradually separate, which indicates that the evaporation rate becomes sensitive to both temperature and pressure. This region represents the shift from surface reaction control to diffusion control and serves as a critical window for process optimization. This phenomenon is a common characteristic feature of metal evaporation under vacuum conditions and is observed for elements such as selenium, tellurium, lead, silver, and antimony. The evaporation rate curves can be described in Logistic model, as shown in Eq. (3):

$$\omega = \frac{A_1 - A_2}{1 + (p/p_0)^m} + A_2 \tag{3}$$

where p is the system pressure, Pa; A_1, A_2, p_0 and m are constants. For each function at different temperatures, the value of the squared correlation coefficient is large (R^2>0.980) and indicates a high degree of accuracy in the fitting parameters and standard curves, as listed in Table 2. At each temperature, the squared correlation coefficient (R^2>0.980) indicates an exceptional level of precision in the fitting parameters and the generated standard curves. The results highlight the robustness

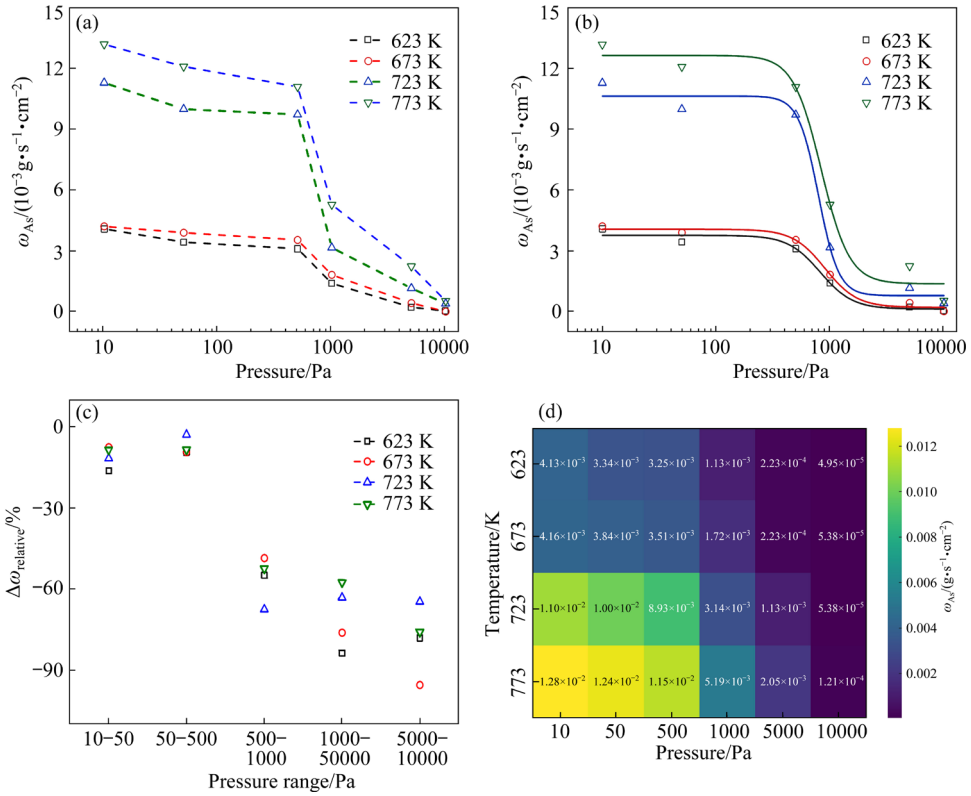

Fig. 5 (a) Plots of evaporation rate of As vs system pressure at different temperatures, (b) Logistic model of evaporation rate curves, (c) relative change in ω_{As} in different pressure ranges, and (d) heatmap of ω_{As} at various temperatures and pressures

Table 2 Fitted values of A_1, A_2, p_0 and m at different temperatures

Temperature/K	A_1	A_2	p_0/Pa	m	Squared correlation coefficient, R^2
623	3.82×10^{-3}	-1.85×10^{-4}	3.744	6.643	0.987
673	4.09×10^{-3}	-2.58×10^{-4}	3.936	7.057	0.980
723	1.07×10^{-2}	6.06×10^{-4}	3.644	11.182	0.994
773	1.28×10^{-2}	2.16×10^{-4}	3.825	6.958	0.987

and reliability of the Logistic model (Fig. 5(b)) in capturing the underlying evaporation behavior.

To better elucidate the effect of pressure on the evaporation behavior of arsenic, the relative change in the evaporation rate ($\Delta\omega_{\text{relative}}$) is calculated for different pressure ranges and temperatures. The relative change was determined using Eq. (4):

$$\Delta\omega_{\text{relative}} = \frac{\omega_{\text{final}} - \omega_{\text{initial}}}{\omega_{\text{initial}}} \tag{4}$$

where ω_{final} and ω_{initial} are the evaporation rates at the final pressure and initial pressure, respectively, of each pressure range.

As shown in Fig. 5(c), the $\Delta\omega_{\text{relative}}$ decreases significantly as the pressure increases, particularly in the low-pressure range (10−500 Pa), where the rate sharply decreases. At higher pressures (>1000 Pa), the relative change become less pronounced, indicating a transition in the controlling mechanism from surface reaction control to diffusion control. Furthermore, higher temperatures reduce the sensitivity of the evaporation rate to pressure changes, highlighting the dominant role of temperature in driving the volatilization process at high pressures. The increased volatility at lower pressures is likely caused by reduced collision frequencies among gas molecules, which minimizes the recondensation or collisional loss of arsenic vapor molecules during the volatilization process and allows a greater number of arsenic molecules to successfully transition into the gaseous phase. The heatmap in Fig. 5(d) shows the variation in arsenic evaporation rates as a function of system pressure and temperature. The dark blue areas indicate low evaporation rates and are distributed predominantly in the low-temperature (640−680 K) and high-pressure (>5000 Pa) regions. In contrast, the light yellow areas indicate high evaporation rates and are concentrated in the high-temperature (>740 K) and low-pressure (<500 Pa) regions; these areas represent the optimal conditions for volatilization. In the intermediate pressure range of 100−500 Pa, the evaporation rate smoothly transitions from high to low, further confirming that this region is a critical point for the mechanism shift.

3.4 Critical pressures, maximum evaporation rates and evaporation coefficients

A common feature of the evaporation of metals under vacuum conditions is that the evaporation rate reaches a maximum and does not significantly change when the system pressure decreases to the critical pressure (p_{crit}). As shown in Fig. 5(b), arsenic also follows the same pattern. The volatilization of arsenic clearly transitions from surface reaction-controlled kinetics at low pressures to diffusion-controlled behavior at high pressures. This transition is characterized by critical pressure regions where both mechanisms interact. The critical pressures of arsenic at different distillation temperatures are plotted by the tangent drawing method and are shown in Fig. 5(b). The maximum evaporation rates of arsenic at different distillation temperatures are determined by calculating the limit of the logistic model, where A_1 represents the actual maximum evaporation rate of arsenic ($\omega_{\text{max,actual}}$), as shown in Eq. (5). Additionally, the theoretical maximum evaporation rate ($\omega_{\text{max,theo}}$) is calculated using the Langmuir equation, as expressed in Eq. (6). In this equation, p^* denotes the saturation vapor pressure of arsenic and is calculated via the Clausius−Clapeyron equation (Pa), M is the relative molecular mass of arsenic (75 g/mol), and T' represents the surface temperature of the melt (K). Notably, the theoretical maximum evaporation rate is several orders of magnitude higher than the experimentally observed value. This discrepancy is quantified by the evaporation coefficient (α) by Eq. (7). The results for the critical pressure, maximum evaporation rate, theoretical maximum evaporation rate and evaporation coefficient are summarized in Table 3. Table 3 shows that the theoretical maximum evaporation rate is several orders of magnitude higher than the experimental value due to various nonideal factors, including molecular size, intermolecular forces, vapor-phase molecular collisions, temperature gradients, and other kinetic limitations of the actual evaporation process.

$$\omega_{\text{max,actual}} = \lim_{p\to 0}\left[\frac{A_1 - A_2}{1+(p/p_0)^m} + A_2\right] = A_1 \tag{5}$$

$$\omega_{\text{max,theo}} = 4.37\times10^{-4}\, p^*\sqrt{M/T'} \tag{6}$$

$$\alpha = \frac{\omega_{\text{max,actual}}}{\omega_{\text{max,theo}}} \tag{7}$$

To better highlight the unique volatilization characteristics of arsenic, a comparative summary of its kinetic parameters with those of Sb and Se is provided in Table 4. Compared with other elements, arsenic has a moderate critical pressure and evaporation rate but a relatively lower evaporation

Table 3 Critical pressure, actual maximum evaporation rate ($\omega_{max,actual}$), theoretical maximum evaporation rate ($\omega_{max,theo}$) and evaporation coefficient (α) of arsenic at different temperatures

Temperature/K	Critical pressure/Pa	$\omega_{max,actual}$/(g·s^{-1}·cm^{-2})	$\omega_{max,theo}$/(g·s^{-1}·cm^{-2})	Evaporation coefficient, α
623	281	3.82×10^{-3}	171×10^{-2}	0.223
673	363	4.09×10^{-3}	8.93×10^{-2}	0.046
723	403	1.07×10^{-2}	3.70×10^{-1}	0.029
773	478	1.28×10^{-2}	1.27	0.01

Table 4 Comparison of volatilization parameters of As, Sb and Se

Element	Temperature range/K	p_{crit}/Pa	ω_{max}/(g·s^{-1}·cm^{-2})	α	Source
As	623−773	281−478	3.82×10^{-3}−1.28×10^{-2}	0.01−0.223	This work
Sb	823−1023	17.54−61.68	0.52−2.81	0.14−0.8	Ref. [14]
Se	523−723	5.34−37.06	2.955×10^{-4}−1.18×10^{-2}	0.0039−0.0363	Ref. [17]

coefficient, indicating the combined effects of its molecular properties and stronger intermolecular interactions under vacuum conditions.

4 Conclusions

(1) The evaporation rate of arsenic is determined at 623−773 K and 10−10000 Pa, which significantly increases with increasing temperature and decreasing pressure. Surface reaction control dominates the volatilization process at low pressures (<100 Pa), whereas diffusion control becomes significant at high pressures (>5000 Pa).

(2) An Arrhenius-type model is established to describe the temperature dependence, and a Logistic model is applied to representing the pressure dependence. The volatilization kinetics and critical parameters, including the activation energy, preexponential factor, critical pressure, maximum evaporation rate, and evaporation coefficient, are determined.

(3) These findings elucidate the volatilization mechanism of arsenic quantitatively and provide theoretical guidance for optimizing industrial vacuum distillation processes at low pressures and high temperatures.

CRediT authorship contribution statement

Lin ZOU: Conceptualization, Methodology, Investigation, Writing − Original draft, Writing − Review & editing; **Guo-long CHEN:** Investigation, Data curation; **Guo-zheng ZHA:** Conceptualization, Methodology, Writing − Review & editing, Project administration; **Wen-long JIANG:** Conceptualization, Methodology, Writing − Review & editing, Project administration; **Bao-qiang XU:** Project administration, Funding acquisition, Resources; **Bin YANG:** Resources, Funding acquisition; **Da-chun LIU:** Resources, Funding acquisition.

Declaration of competing interest

The authors declare that they have no known competing financial interests or personal relationships that could have appeared to influence the work reported in this paper.

Acknowledgments

The authors express their sincere appreciation for Yunnan Fundamental Research Project, China (No. 202201BE070001-056).

References

[1] STOCK T J Z, WARSCHKOW O, CONSTANTINOU P C, BOWLER D R, SCHOFIELD S R, CURSON N J. Single-atom control of arsenic incorporation in silicon for high-yield artificial lattice fabrication [J]. Advanced Materials, 2024, 36: 2312282. https://doi.org/10.1002/adma.202312282.

[2] JAIN N, SINGH P, BHATNAGAR A, MAITI A. Arsenite oxidation and adsorptive arsenic removal from contaminated water: a review [J]. Environmental Science and Pollution Research, 2024, 31: 42574−42592. https://doi.org/10.1007/s11356-024-33963-x.

[3] CHANGOTRA R, RAJPUT H, LIU B, MURRAY G, HE Q. Occurrence, fate, and potential impacts of wood preservatives in the environment: Challenges and environmentally friendly solutions [J]. Chemosphere, 2024, 352: 141291. https://doi.org/10.1016/ j.chemosphere.2024.141291.

[4] SEVAK P, PUSHKAR B. Arsenic pollution cycle, toxicity and sustainable remediation technologies: A comprehensive review and bibliometric analysis [J]. Journal of Environmental Management, 2024, 349: 119504. https://doi.org/10.1016/j.jenvman.2023.119504.

[5] TYLER C R, ALLAN A M. The effects of arsenic exposure on neurological and cognitive dysfunction in human and rodent studies: A review [J]. Current Environmental Health

Reports, 2014, 1: 132−147. https://doi.org/10.1007/s40572-014-0012-1.
[6] XUE Jian-rong, LONG Dong-ping, ZHONG Hong, WANG Shuai, LIU Li-hua. Comprehensive recovery of arsenic and antimony from arsenic-rich copper smelter dust [J]. Journal of Hazardous Materials, 2021, 413: 125365. https://doi.org/10.1016/j.jhazmat.2021.125365.
[7] LONG Hua, HUANG Xing-zhong, ZHENG Ya-jie, PENG Ying-lin, HE Han-bing. Purification of crude As_2O_3 recovered from antimony smelting arsenic-alkali residue [J]. Process Safety and Environmental Protection, 2020, 139: 201−209. https://doi.org/10.1016/ j.psep.2020.04.015.
[8] ZHANG Huan, ZHANG Wei, CAO Pan, LI Yi-fu, YANG Bin, CHEN Xiu-min, XU Bao-qiang. Clean and sustainable elimination of arsenic–aluminum slag from smelted crude tin via vacuum volatilization – Fractional condensation [J]. Journal of Cleaner Production, 2024, 452: 142212. https://doi.org/10.1016/ j.jclepro.2024.142212.
[9] ZHANG Xiao-xin, FRIEDRICH S, FRIEDRICH B. Separation behavior of arsenic and lead from antimony during vacuum distillation and zone refining [J]. Journal of Materials Research and Technology, 2020, 9: 4386−4398. https://doi.org/10.1016/j.jmrt.2020.02.063.
[10] WANG Wei. Experimental study on vacuum distillation pre purification of crude (metallic) arsenic [J]. Yunnan Metallurgy, 2010, 39(5): 30−34. (in Chinese). https://doi.org/10.3969/j.issn.1006-0308.2010.05.006.
[11] ZHANG Huan, LI Yi-fu, CHEN Xiu-min, YANG Bin, XU Bao-qiang. Sustainable and green removal of arsenic from crude tin via vacuum gasification–directional condensation [J]. Separation and Purification Technology, 2024, 351: 128139. https://doi.org/10.1016/ j.seppur.2024.128139.
[12] PU Zheng-hao, LI Yi-fu, ZHANG Huan, XU Jun-jie, YANG Bin. A new method for separation of As−Pb alloys: Vacuum distillation-condensation [J]. Vacuum, 2019, 166: 140−146. https://doi.org/10.1016/j.vacuum.2019.05.007.
[13] PENG Zhi-qiang, LIAO Ya-long, ZHOU Juan. Review and trend of preparation of high purity arsenic [J]. CIESC Journal, 2013, 32(12): 2929. https://doi.org/10.3969/j.issn.1000-6613.2013.12.023.
[14] YANG Zhen, DENG Tong-da, LUO Huan, LEI Xian-jun, XU Bao-qiang, JIANG Wen-long, YANG Bin. Removal of arsenic and recovery of tin from arsenic-containing multi-metallic materials by vacuum reduction roasting [J]. Vacuum, 2024, 226: 113332. https://doi.org/10.1016/ j.vacuum.2024.113332
[15] MENG Chao-song, YANG Huan, WEI Xiao-hui, XIONG Heng, DONG Zhao-wang, YANG Bin, XU Bao-qiang, WU Xiao-song, TANG Zhao-hui, HE Yu-hong. Evaporation rate and kinetic mechanism of noble antimony under vacuum [J]. Separation and Purification Technology, 2025, 352: 128235. https://doi.org/10.1016/ j.seppur.2024.128235.
[16] GUO Xin-yu, ZHAO Yun, ZHA Guo-zheng, WANG Jia-hao, JIANG Wen-long, YANG Bin, MA Wen-hui. Research of the evaporation law of elemental antimony under vacuum [J]. Vacuum, 2022, 200: 110985. https://doi.org/10.1016/j.vacuum.2022.110985.
[17] ZHAO Yun, GUO Xin-yu, JIANG Wen-long, LI Bao-le, ZHA Guo-zheng, YANG Bin, XU Bao-qiang. Investigation of the evaporation kinetics of a lead−silver alloy and elementary substances under vacuum [J]. Vacuum, 2022, 195: 110670. https://doi.org/10.1016/ j.vacuum.2021.110670.
[18] ZHA Guo-zheng, ZHAO Yun, LUO Huan, JIANG Wen-long, XU Bao-qiang, YANG Bin. Evaporation regularities of elemental selenium in the vacuum distillation process [J]. Metallurgical and Materials Transactions B, 2022, 53: 3856−3864. https://doi.org/10.1007/s11663-022-02647-7.
[19] JIANG Zong-kui, YU Hao-song, TIAN Yang, YANG Bin, XU Bao-qiang, KONG Ling-xin, LIANG Dong, ZHANG Jia-peng. Investigation of arsenic removal from industrial yellow phosphorus through vacuum distillation: Thermodynamic and ab initio molecular dynamics [J]. Separation and Purification Technology, 2024, 334: 126067. https://doi.org/10.1016/j.seppur.2023.126067.
[20] ZHENG Yong-xing, HU Pan-jin, LV Jin-fang, XIONG Heng, LAI Zhen-ning. Separation of arsenic and tin from Cu−As alloy based on phase transformation in a vacuum to form Cu−Fe−S compounds [J]. Journal of Alloys and Compounds, 2021, 886: 161267. https://doi.org/10.1016/j.jallcom.2021. 161267.

砷在真空蒸馏过程中的挥发动力学和机理

邹 琳[1,2,3]，陈国龙[1,2]，查国正[1,2]，蒋文龙[1,2]，徐宝强[1,2]，杨 斌[1,2]，刘大春[1,2]

1. 昆明理工大学 真空冶金国家工程研究中心，昆明 650093；
2. 昆明理工大学 冶金与能源工程学院，昆明 650093；
3. 山东恒邦冶炼股份有限公司，烟台 264000

摘 要：研究了在 623~773 K 和 10~10000 Pa 条件下砷的挥发特性和动力学机制。结果表明，砷的蒸发速率随温度升高和系统压力降低而增加。在低压条件下(<100 Pa)蒸发过程主要受表面反应控制，而在高压条件下(>5000 Pa)扩散控制占主导地位。蒸发行为可分别通过温度依赖性的 Arrhenius 模型与压力依赖性的 Logistic 模型精确描述。获得了临界压力、最大蒸发速率与蒸发系数关键动力学参数。其中，蒸发系数在 0.010~0.223 之间，临界压力随温度在 281~478 Pa 范围内变化。

关键词：砷；真空蒸馏；蒸发速率；动力学模型；工艺优化

(Edited by Bing YANG)